

# A predictive model for fling-step in near-fault ground motions based on recordings and simulations

Lynne S. Burks\*, Jack W. Baker

*Department of Civil and Environmental Engineering, Stanford University, Stanford, CA 94305-3013, USA*

---

## Abstract

We identify potential data sources for fling-step and discuss their value, compile a dataset of simulated and recorded ground motions containing fling, extract fling pulses from these ground motions, and derive a predictive model for fling amplitude and period that is compared to existing empirical models. Fling is the result of permanent static offset of the ground during an earthquake, but is usually ignored because ground motion records from accelerometers contain errors that make it difficult to measure static offsets. However, some data sources include fling, such as specially processed recordings, ground motion simulations, and high-rate global positioning systems (GPS). From this data, we extract fling pulses using the pattern search global optimization algorithm. The resulting displacement amplitudes and periods are used to create a new predictive equation for fling parameters, are compared to existing empirical models for pulse period, fling amplitude, and surface displacement along the fault, and are found to match reasonably well.

*Keywords:* near-fault, fling-step, pulse-like, ground motion simulations

---

## 1. Introduction

Fling-step is the result of elastic rebound theory, when stress and displacement slowly build up in the earth's crust over long periods of time and then are suddenly released, causing a large permanent ground displacement

---

\*Corresponding author. Tel.: +1-314-570-6721

*Email address:* lynne.burks@alumni.stanford.edu (Lynne S. Burks)

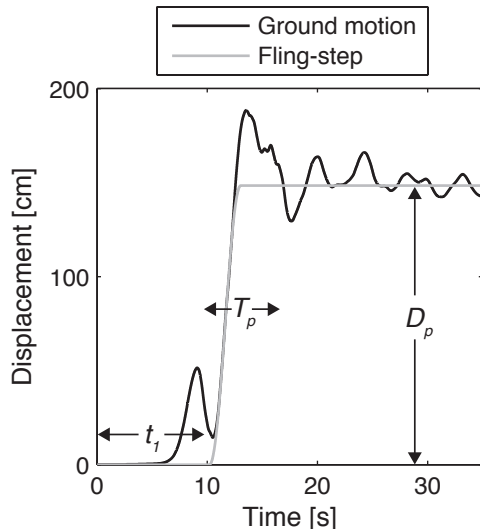


Figure 1: Ground motion that clearly shows fling-step (i.e., static offset) from the YPT-N/S station in the 1999 Kocaeli, Turkey earthquake, where  $D_p$  is the displacement amplitude,  $T_p$  is the period or duration, and  $t_1$  is the arrival time.

in a matter of seconds [1] (e.g., Figure 1). This permanent displacement causes a long-period pulse that is distinct from the more familiar directivity pulse, which is caused by the constructive interference of propagating seismic waves. Until the Chi-Chi, Taiwan and Kocaeli, Turkey earthquakes in 1999, fling went largely unnoticed because the long-period energy of prior earthquakes was dominated by directivity effects [1]. In addition, the static offset caused by fling is typically removed from ground motion records via processing (generally a combination of filtering and baseline correction), which is used to remove noise and errors due to baseline offsets [2].

In general, the use of processed ground motions, and thus the neglect of fling's static offset, for engineering applications is considered acceptable because baseline correction has a negligible effect on elastic spectral response at periods of engineering interest [3, 4]. However, near-fault ground motions containing directivity or fling pulses consistently increase the seismic demand on nonlinear structures compared to far-field motions [5, 6]. Due to the lack of recorded ground motions containing fling, the cited studies use idealized fling pulses modeled as trigonometric functions in addition to small sets of baseline corrected ground motions.

This lack of data on fling leads to a lack of predictive models for fling parameters, such as displacement amplitude and period (i.e., duration). The only published predictive models for fling parameters are the Abrahamson [7] model and the recently published Kamai et al. [8] model. The addition of the predictive model presented in this paper will help quantify the epistemic uncertainty associated with fling parameters. However, the full uncertainty associated with fling will remain large because similar to existing fling models, the proposed model is largely based on ground motion simulations.

Here we address the lack of fling data in the engineering community by evaluating potential data sources, extracting fling pulses from existing data sources, and deriving a predictive model for fling parameters that is then compared to current empirical models. We compile a dataset of ground motions containing fling which consists of 67 specially processed recordings, 44 high-rate GPS recordings, and almost 2.2 million ground motion simulations. One of the most valuable potential sources for fling data is ground motion simulations, which enable the relatively quick collection of a large dataset and are free of noise, so no processing is required.

## 2. Data sources for fling

Historically, the dynamic component of fling has been difficult to measure because of noise and lack of precision in recording instruments. The static component of fling has been measured using interferometric synthetic aperture radar (InSAR) and global positioning systems (GPS) [e.g., 9, 10], but these data sources do not capture the period of fling, which is important for the dynamic response of structures.

More recent sources of data, such as ground motion simulations and high-rate GPS, capture both the static and dynamic component of fling. The following sections describe the potential data sources for dynamic fling-step, including their usefulness and pervasiveness in the engineering community. For a more detailed description of these data sources, see [11].

### 2.1. Libraries of processed ground motion records

Unprocessed ground motion records are taken straight from an accelerometer and typically contain errors due to noise or baseline offsets caused by tilting or transducer response to sharp pulses in the ground motion. It is common for small baseline offsets to cause an unrealistic linear increase in velocity with time and a quadratic increase in displacement. To correct for

these errors, records are typically processed via filtering and/or baseline correction before being placed in a library of strong motion records.

Many libraries of strong ground motions exist to aid engineers in ground motion selection, such as the Pacific Earthquake Engineering Research Center (PEER) Next Generation Attenuation (NGA) database [12, 13], the Center for Engineering Strong Motion Data (CESMD) [14, 15], the European Strong Motion Database (ESD) [16], and the Italian Accelerometric Archive (ITACA) [17, 18]. Out of these databases, only the Lucerne station from the 1992 Landers earthquake in the PEER NGA database contains a static offset because it was one of the earliest near-fault recordings to contain both directivity and fling, and was therefore specially processed [19]. All other ground motions are processed in a way that removes static displacements (and some databases contain unprocessed versions of ground motions as well). These databases are thus not very useful for engineers who want to include fling in their analysis. Also, any engineer who selects ground motions from these databases neglects fling’s static displacement by default.

## *2.2. Specially processed ground motion records*

Special processing techniques, such as baseline correction, can be used to preserve static offsets by subtracting a bilinear, trilinear, or parabolic baseline from the velocity time history and forcing the velocity to integrate to a constant displacement [20, 3]. However, the results of baseline correction can be highly dependent on the choice of baseline, and unless the actual static offset is known from another data source such as GPS or InSAR, the final baseline corrected record can vary widely. This uncertainty is one reason why ground motions in engineering databases are processed using both baseline correction and filtering, resulting in the loss of static offsets. But with improvements to digital accelerometers and GPS technology, it is becoming more feasible to recover static offsets using a modified version of baseline correction [21].

We baseline corrected or obtained existing baseline corrected versions of ground motion records from several large earthquakes known to have produced static offsets, including 1999 Chi-Chi, Taiwan (Figure 2); and one station from each of the following: 1999 Kocaeli, Turkey; 2002 Denali, Alaska, USA; and 2010 Darfield, New Zealand using the procedure outlined in Boore [3] and Wu and Wu [21]. The baseline corrected ground motions can be downloaded here: <http://purl.stanford.edu/pz055cs5875>.

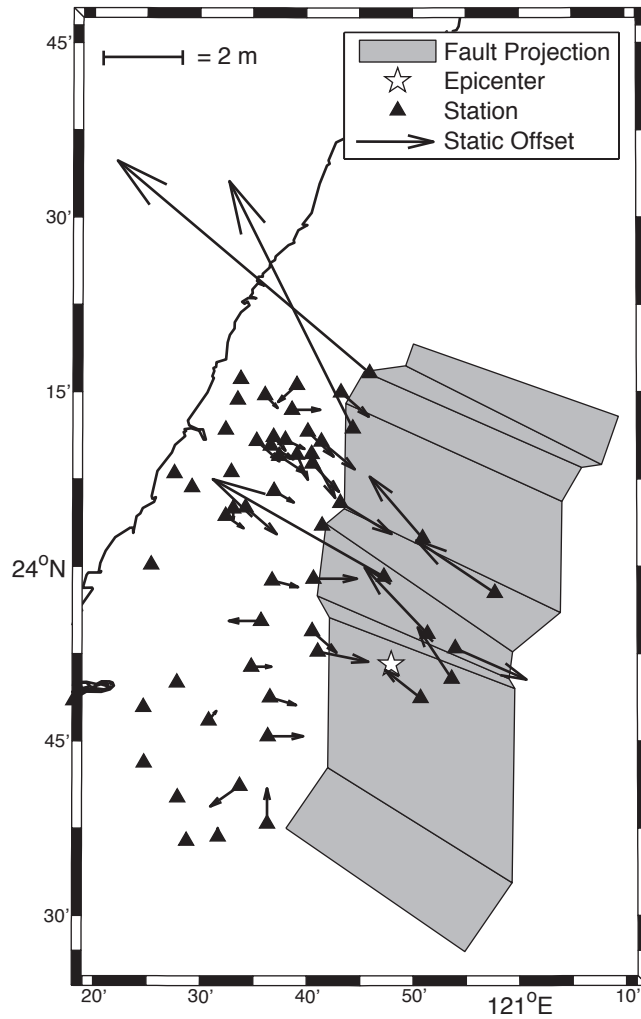


Figure 2: Static offsets of the ground following the 1999 Chi-Chi, Taiwan, earthquake. The direction of arrows indicates direction of displacement, and length of arrows indicates relative amplitude of displacement.

### 2.3. Ground motion simulations

Many methods exist for simulating ground motions, such as stochastic-process-based methods, finite-fault methods, kinematic methods, and hybrid methods. For a comprehensive review of ground motion prediction techniques, see, for example, [11, 22]. Here we focus on kinematic and hybrid simulations because these methods include earthquake source and wave propagation path information and therefore directly model fling-step.

In this study, we used three sets of ground motion simulations: (1) kinematic simulations of earthquake scenarios similar to the 1906 San Francisco earthquake, referred to as “SF scenarios” [23, 24], (2) kinematic simulations of earthquake scenarios on the Hayward fault, referred to as “Hayward scenarios” [25, 26], and (3) hybrid broadband simulations of earthquake scenarios on generic reverse faults, referred to as “reverse scenarios” (Albert Kottke, personal communication, February 2012).

The SF and Hayward scenarios were computed by several different research groups, but only those computed by Aagaard are used in this study due to their availability. These simulations consist of low-frequency seismograms with a maximum frequency of 0.5 Hz and were computed using a finite-element wave propagation scheme. The SF scenarios consist of 6 earthquake scenarios with rupture geometry similar to the 1906 San Francisco earthquake and varying slip distributions and hypocenter locations, and each scenario contains simulated time histories at more than 35,000 sites around the San Andreas fault (Figure 3). The Hayward scenarios consist of 29 earthquake scenarios on the Hayward fault with varying magnitudes, fault dimensions, and hypocenter locations, and each scenario contains simulated time histories at more than 60,000 sites.

The reverse scenarios are hybrid broadband simulations computed using the Graves and Pitarka [27] hybrid broadband method on the Southern California Earthquake Center (SCEC) Broadband Platform (BBP), which is an open-source software package that includes simulation codes from multiple researchers and allows user-defined source and site characteristics [28]. The reverse scenarios consist of 40 different earthquake scenarios with varying magnitude (from 6 to 7.5), dip (from 20 to 70 degrees), and depth to rupture (0 to 5 km). Each scenario was realized 30 times with a different slip distribution, resulting in a total of 1,200 simulated earthquakes. Static offsets are preserved in all these simulations, and fling-step is clearly observed in some displacement time histories.

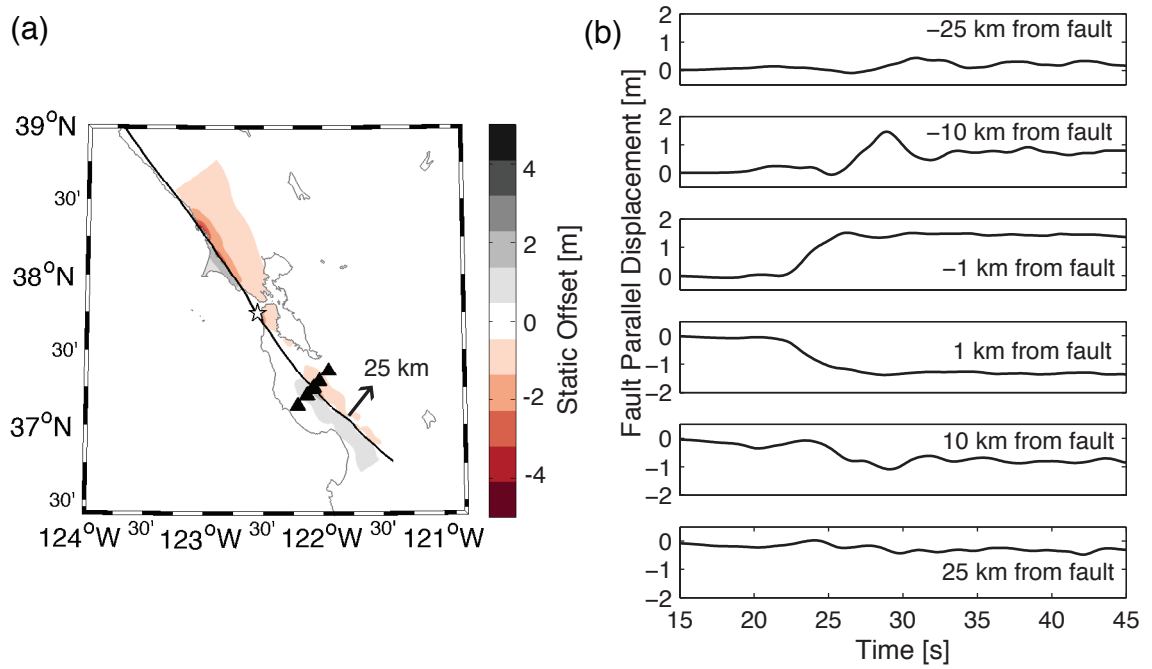


Figure 3: Example SF scenario: (a) map of the static offsets in the fault-parallel direction, and (b) sample displacement time histories. Black triangles on the map are the stations for which time histories are plotted and white star is the epicenter.

#### 2.4. High-rate GPS

High-rate global positioning systems (GPS) are a relatively new technology that use GPS instruments to record the location of a station at a sampling rate of 1 to 10 Hz, obtaining a crude displacement time history of seismic events. This technology is more frequently used in seismology than engineering, with many studies using GPS data to recover the source slip function [e.g., 29, 30]. Some studies focus on combining the results from high-rate GPS with a traditional accelerometer to obtain more accurate displacement time histories, and results are available for the 2003 Tokachi-Oki, Japan earthquake [31] and the 2010 El Mayor-Cucapah, Mexico earthquake [32]. Unfortunately for this study, most of the displacement time histories from high-rate GPS are located far from the source or have very small static offsets, limiting their value for engineering studies. However, we still use high-rate GPS ground motions in the following sections to evaluate fling characteristics at large distances. Despite its current lack of data for the purposes of this study, high-rate GPS has the potential to produce valuable data in the future.

### 3. Extracting fling from a ground motion time history

The defining characteristic of fling is the static displacement at the end of the record, which can be represented by a ramp function fit to a displacement time history. We use the following equation to define fling, based on its good match to observed displacement time histories (see Figure 1):

$$d(t) = \frac{D_p}{2} \sin \left[ \frac{\pi}{T_p} \left( t - t_1 - \frac{T_p}{2} \right) \right] + \frac{D_p}{2} \quad t_1 \leq t \leq T_p + t_1 \quad (1)$$

where  $d(t)$  is the displacement as a function of time,  $D_p$  is the maximum displacement amplitude of the pulse,  $T_p$  is the period or duration of the pulse, and  $t_1$  is the arrival time.

To study fling in ground motions, the three fling parameters that define equation 1 (i.e.,  $D_p$ ,  $T_p$ , and  $t_1$ ) must be extracted from a displacement time history. The value of  $D_p$  can simply be defined as the displacement at the end of the ground motion, but choosing the “best” values for  $T_p$  and  $t_1$  is not so straightforward. Therefore the pattern search global optimization algorithm [33] was used to minimize the sum of squared error between each ground motion displacement in our dataset and equation 1 (see [11] for more

Table 1: Historical ground motion recordings in our dataset, along with their minimum and maximum displacement,  $D_p$ . (For earthquakes with one station, the min. and max.  $D_p$  are in orthogonal orientations.)

EQ Name	Year	$M_w$	# Stations	Min. $D_p$ (cm)	Max. $D_p$ (cm)
Landers	1992	7.3	1	109.4	167.7
Kocaeli	1999	7.5	1	117.5	148.4
Chi-Chi	1999	7.6	63	17.5	652.2
Denali	2002	7.9	1	80.1	176.0
Tokachi-Oki	2003	8.3	37	5.6	56.6
Darfield	2010	7.0	1	95.8	136.2
El Mayor-Cucapah	2010	7.2	7	5.1	17.9

details). Fling parameters were extracted from each ground motion in the fault normal and fault parallel components.

Our dataset consists of all ground motions described in Section 2, which includes simulations from the SF, Hayward, and reverse scenarios; the Lucerne station from Landers in the PEER NGA database; baseline corrected ground motions of multiple stations from Chi-Chi, the YPT station from Kocaeli, Pump Station 10 from Denali, and the GDLC station from Darfield; and high-rate GPS combined with traditional accelerometer recordings from Tokachi-Oki and El Mayor-Cucapah (Table 1).

#### 4. Predictive model for fling parameters

We derive a predictive model for fling period and amplitude using the extracted fling parameters (i.e.,  $T_p$  and  $D_p$ ) from the previous section, and evaluate it through comparison with relevant empirical models. There are only two empirical models created explicitly for fling [7, 8], but other models are applicable such as models for pulse period as a function of earthquake magnitude [e.g., 34, 35], models for surface displacement as a function of distance for the 1906 San Francisco earthquake [e.g., 36], and models for the maximum and average surface displacement near the fault [e.g., 37].

##### 4.1. Fling period

The extracted fling period is compared to empirical predictions for pulse period based on magnitude [e.g., 7, 8, 34, 35]. All these empirical predictions are based on magnitude alone, except Kamai et al. [8] which also depends on

rupture mechanism (e.g., strike-slip or reverse and dip). Seismology theory suggests that pulse period is closely related to the rise time of slip on the fault and the logarithm of rise time is proportional to magnitude, therefore  $\ln T_p$  has a strong linear dependence on magnitude, although with large variability [38, 39].

The fling period is plotted as a function of magnitude for the 100 stations with largest fling amplitude from each SF, Hayward, and reverse scenario and all stations from historical events (i.e., Landers, Chi-Chi, Kocaeli, Denali, Darfield, Tokachi-Oki, and El Mayor-Cucapah) (Figure 4). Using these data, linear regression provides the following equations:

$$\mu_{\ln T_p} = 1.03M - 5.95 \quad (2)$$

$$\sigma_{\ln T_p} = 0.56 \quad (3)$$

where  $M$  is moment magnitude and  $T_p$  is fling period. Hereafter, equations 2 and 3 are referred to as the Burks and Baker model.

The distribution of fling periods is compared to empirical models at several magnitudes: (1)  $M = 7.8$ , using all SF scenarios, (2)  $M = 6.76$ , using a subset of Hayward scenarios, (3)  $M = 7.0$ , using a subset of reverse scenarios, and (4)  $M = 7.6$ , using recordings from Chi-Chi (Figure 5). For each simulated scenario, we included the 100 stations with the largest fling amplitude. No single empirical model provides a clear best fit to the data across all cases.

#### 4.2. Fling amplitude

Here we evaluate the fling amplitude as a function of closest distance to the fault and moment magnitude. Using all SF and Hayward scenarios, specially processed recordings, and high-rate GPS data from Section 2, we derived the following relationship:

$$\ln D_p = \ln (\cot^{-1} (0.3R)) + 1.3M - 5.1 \quad (4)$$

where  $\ln D_p$  is the natural logarithm of the fling amplitude (in cm),  $R$  is the closest distance to the fault (in km), and  $M$  is the moment magnitude. This equation is based on the functional form suggested by Byerley and DeNoyer [36], combined with an approximation of rupture area for strike-slip faults by Wells and Coppersmith [37], and is similar to the prediction provided by

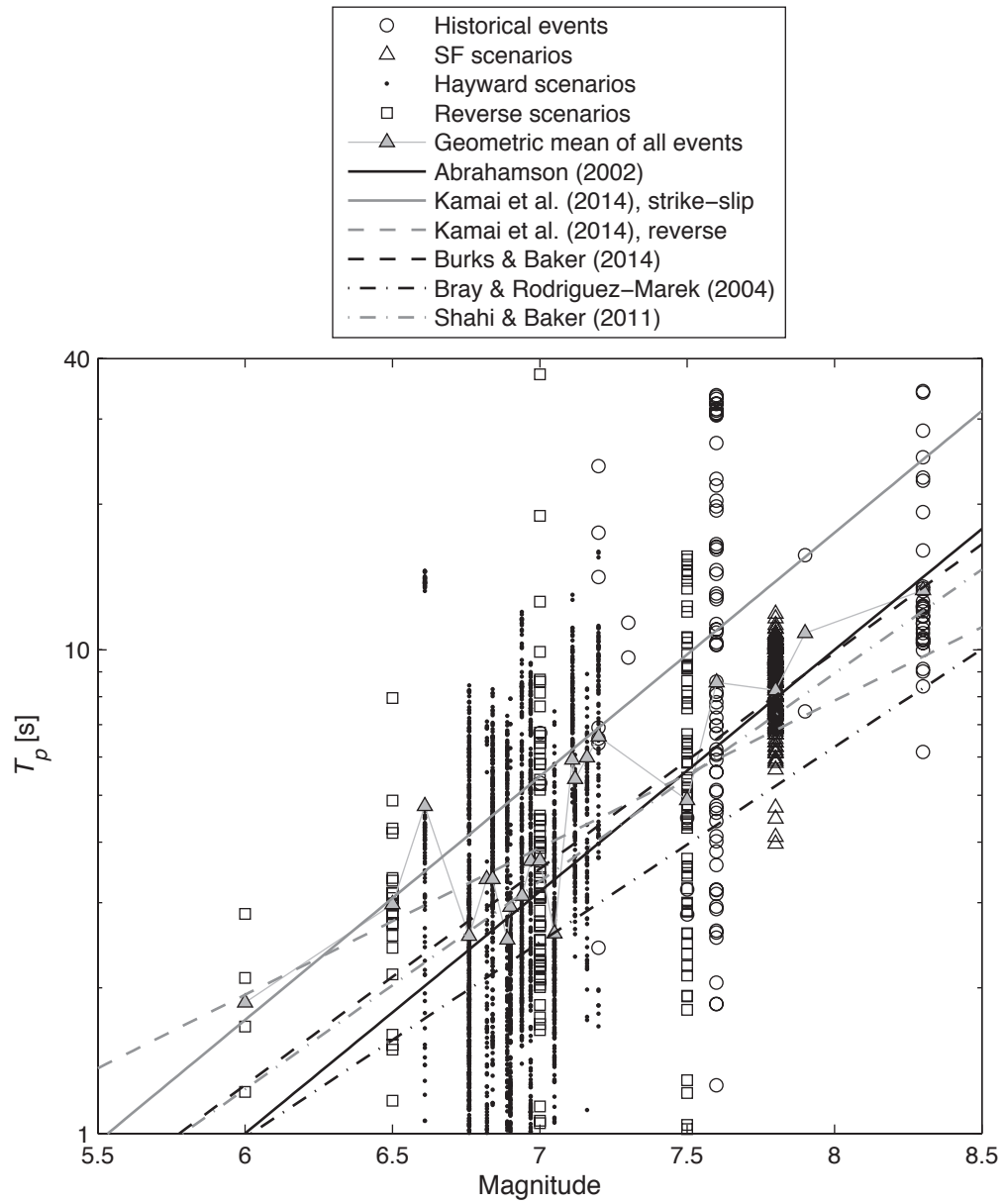


Figure 4: Fling period of ground motions from all historical events (i.e., Landers, Chi-Chi, Kocaeli, Denali, Darfield, Tokachi-Oki, and El Mayor-Cucapah) and a sample of ground motions from SF, Hayward, and reverse scenarios, compared to the median prediction from empirical models.

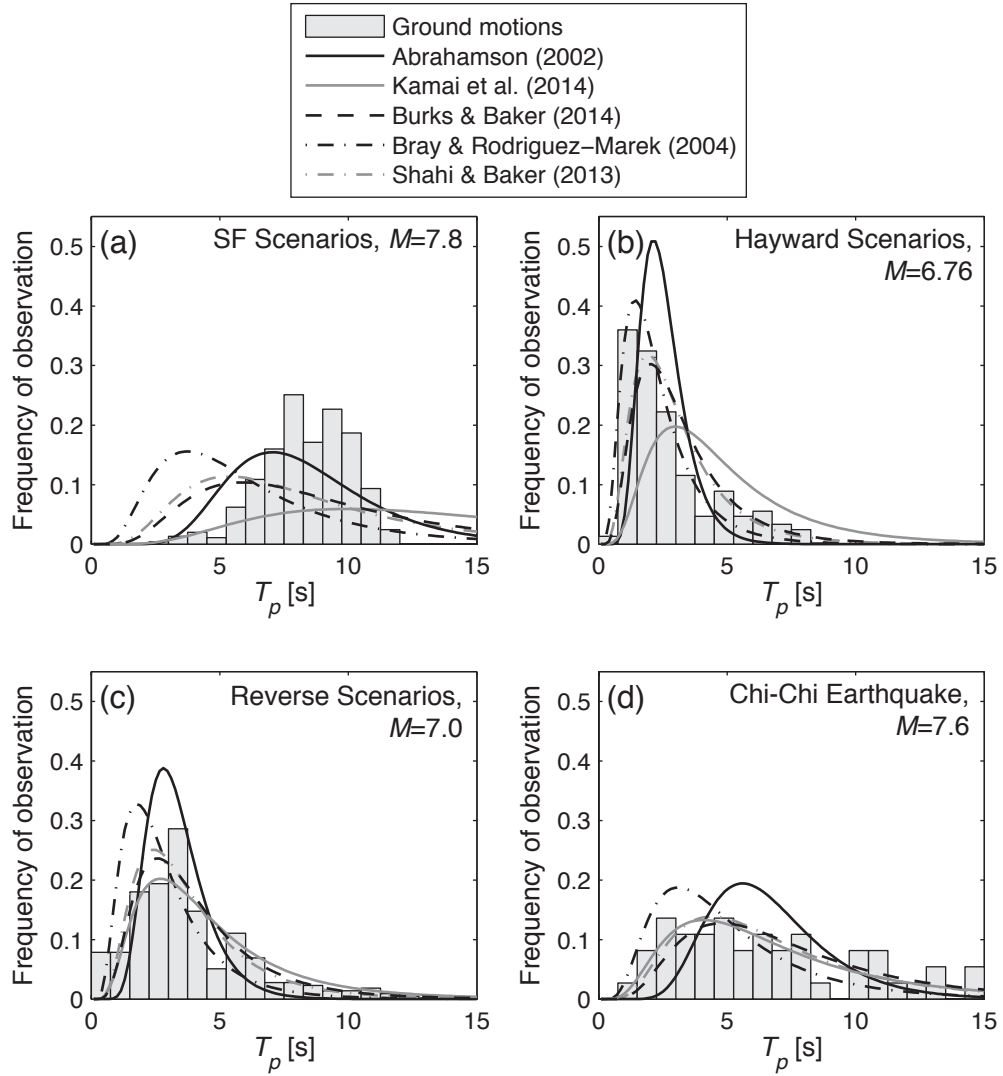


Figure 5: Histogram of fling period from the 100 stations with largest  $D_p$  from (a) SF scenarios,  $M = 7.8$ , (b) subset of Hayward scenarios,  $M = 6.76$ , (c) subset of reverse scenarios,  $M = 7.0$ , and (d) all ground motions from the Chi-Chi earthquake,  $M = 7.6$ , compared to distributions from empirical models.

Abrahamson [7]. The proposed model does not depend on rupture mechanism and dip, as Kamai et al. [8] does, to promote simplicity and ease of use. Hereafter, equation 4 is referred to as the Burks and Baker model.

The smoothed average of fling amplitude for each scenario is compared to relevant empirical models and results from recordings. In Figure 6, each “single scenario” line represents the average fling amplitude of all simulated ground motions in one earthquake scenario as a function of closest distance to the fault.

For the SF scenarios (Figure 6a), fling amplitude is compared to results from recordings, predictions from Byerley and DeNoyer [36] (which only applies to static offsets from the 1906 San Francisco earthquake), and predictions from Abrahamson [7], Kamai et al. [8], and Burks and Baker. All predictive models depend on distance, and the Kamai et al. [8] model also depends on rupture mechanism (e.g., strike-slip or reverse and dip) and the strike-slip model was used here. Some SF scenarios tend to follow Abrahamson [7] and Kamai et al. [8], while others follow Burks and Baker. All ground motions, both simulated and recorded, show a significant amount of scatter. The combined high-rate GPS and accelerometer records from Tokachi-Oki and El Mayor-Cucapah only occur at large distances and relatively small amplitudes.

For the subset of Hayward scenarios (Figure 6b), fling amplitude is compared to predictions for the median magnitude of all Hayward scenarios (i.e.,  $M = 6.9$ ) from Abrahamson [7], the Kamai et al. [8] strike-slip model, Burks and Baker, and results from recordings. The amplitudes from recordings are larger than simulations at all distances because the recordings are from earthquakes with larger magnitudes. For some Hayward scenarios, the smoothed average of  $D_p$  is much smaller than all predictions at distances less than 10 km. This is likely because the Abrahamson [7], Kamai et al. [8], and Burks and Baker models assume a surface-rupturing fault, but for many Hayward scenarios, the rupture does not reach the surface. This highlights the potential value of including a parameter such as depth-to-top of rupture in future predictions of fling amplitude. Also, scenarios with smaller magnitudes tend to result in smaller amplitudes.

For the subset of reverse scenarios (Figure 6c), fling amplitude is compared to predictions for  $M = 7$  from Abrahamson [7], the Kamai et al. [8] reverse model with a dip of 45 degrees, Burks and Baker, and results from recordings. The smoothed average of simulations reasonably match all predictions, which were developed using ground motion simulations similar to

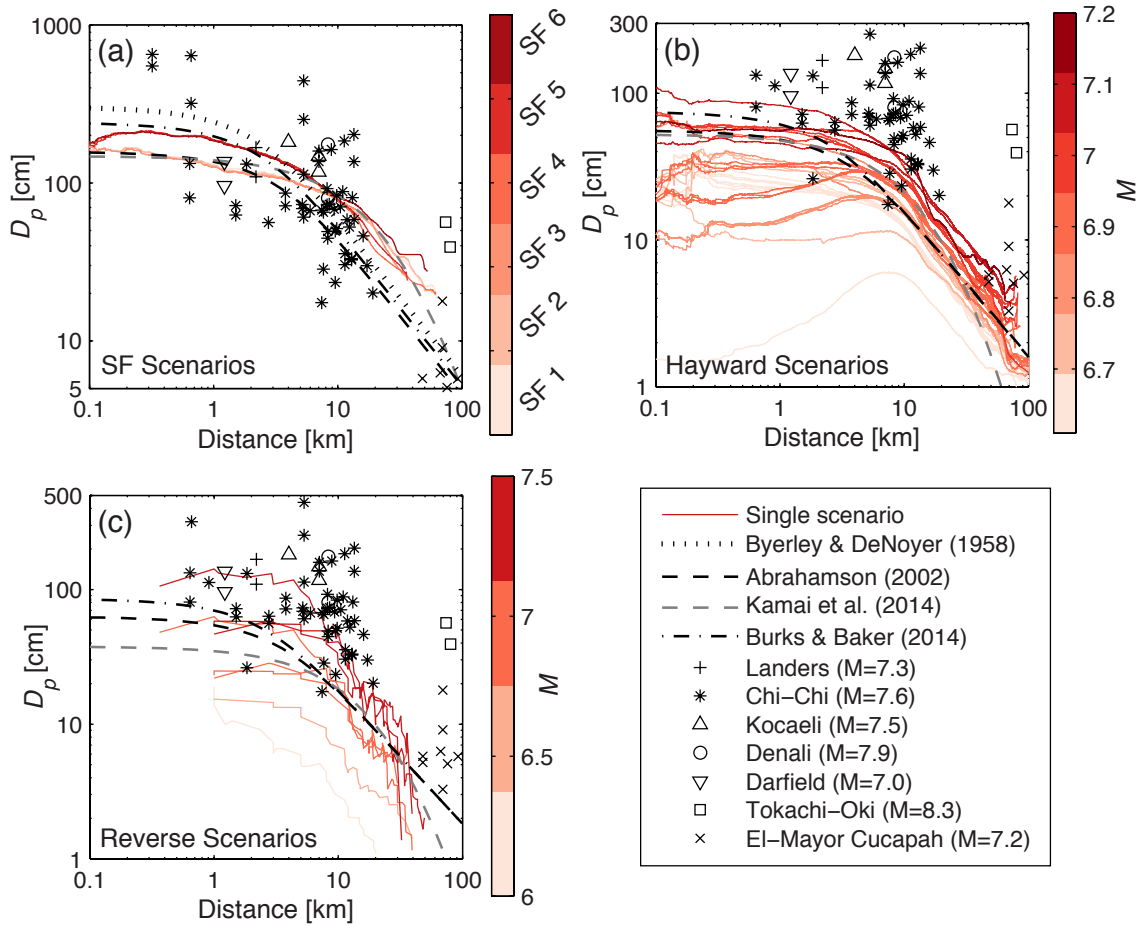


Figure 6: Smoothed average of fling amplitude,  $D_p$ , for all (a) SF scenarios, (b) Hayward scenarios, and (c) reverse scenarios as a function of closest distance to the fault. Some Chi-Chi recordings have have  $D_p > 500\text{cm}$ , and are thus not visible on the figure.

the reverse scenarios. Again, the average amplitudes from simulations are smaller than recordings because the recordings are from larger magnitude earthquakes and simulations with smaller magnitudes tend to have smaller amplitudes.

The average and maximum surface displacement along the fault for each surface-rupturing simulation is shown as a function of earthquake magnitude (Figure 7). The average surface displacement was computed for strike-slip events (i.e., SF and Hayward scenarios) by taking the average absolute static offset from all stations located within 20 m of the fault and for reverse events (i.e., reverse scenarios) by taking the average absolute static offset from the closest stations on the hanging-wall. The results from simulations are compared to empirical predictions from Wells and Coppersmith [37], which provide a median for the average and maximum surface displacement as a function of magnitude, and Abrahamson [7], Kamaï et al. [8], and Burks and Baker, which provide median fling amplitude as a function of magnitude and distance (a distance of 0 km was used for comparison with Wells and Coppersmith [37]). The Wells and Coppersmith [37] and Kamaï et al. [8] models also depend on rupture mechanism (e.g., strike-slip or reverse and dip).

## 5. Conclusions

We identified potential data sources for fling and discussed the value of each source to the engineering community, including libraries of processed ground motions, specially processed ground motions, ground motion simulations, and high-rate GPS. We also compiled an example dataset using ground motions from each source, extracted fling pulses from all ground motions, and derived a predictive model for fling amplitude and period that was compared to existing empirical models. This new predictive model can help quantify the epistemic uncertainty associated with fling parameters.

For ground motion simulations, we used kinematic source simulations of scenarios similar to the 1906 San Francisco earthquake (i.e., SF scenarios) and scenarios on the Hayward fault (i.e., Hayward scenarios), and hybrid broadband simulations of reverse earthquake scenarios (i.e., reverse scenarios). Because the long-period portion of these simulations is deterministically computed using a kinematic source model and wave propagation theory, static offsets are produced, making ground motion simulations an extremely valuable tool for the characterization of fling because they can be generated as needed.

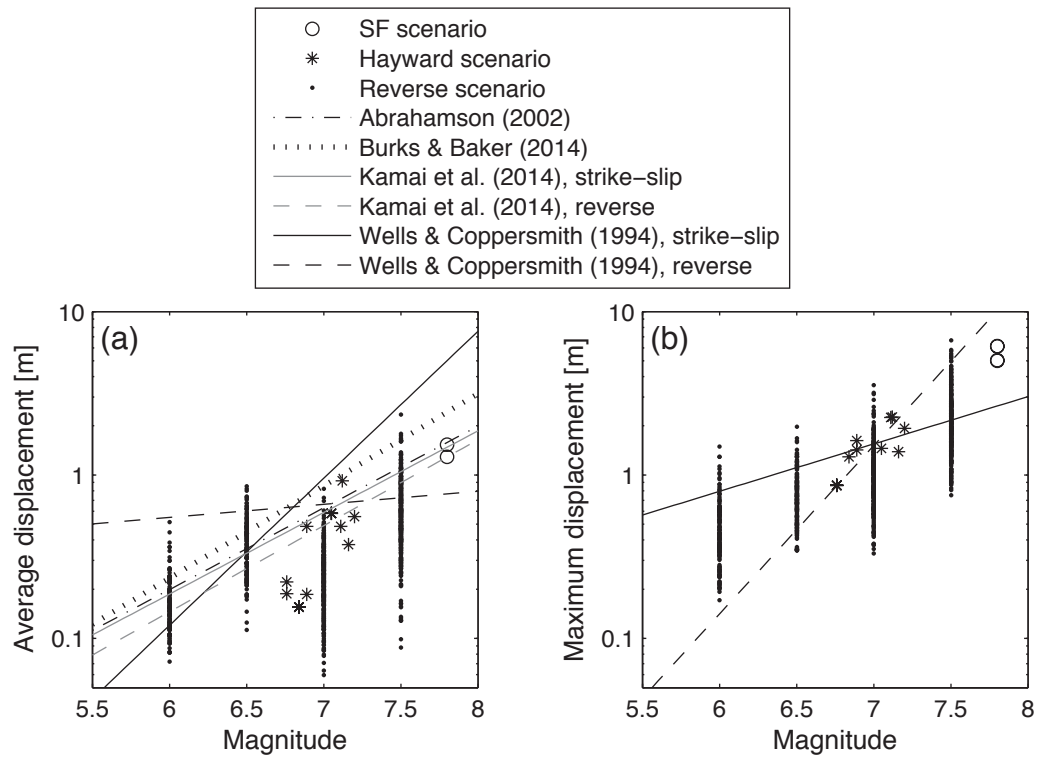


Figure 7: (a) Average and (b) maximum surface displacement along the fault for all surface-rupturing SF, Hayward, and reverse scenarios, compared to the median prediction from empirical models.

For ground motion recordings (e.g., libraries of processed ground motions, specially processed ground motions, and high-rate GPS), data is much more sparse. Recorded ground motions typically contain errors that must be corrected before use in engineering applications, and nearly all ground motions in engineering databases are processed via a combination of filtering and baseline correction that removes all static offsets. Unprocessed ground motions can be corrected using baseline correction only to preserve static offsets. We baseline corrected 63 stations from the 1999 Chi-Chi, Taiwan earthquake; the YPT station from the 1999 Kocaeli, Turkey earthquake; and the GDLC station from the 2010 Darfield, New Zealand earthquake; and the USGS baseline corrected Pump Station 10 from the 2002 Denali, Alaska, USA earthquake. However, this method is rarely used because results are very sensitive to choice of processing parameters. Typical strong motions can also be combined with high-rate GPS recordings, for example from the 2003 Tokachi-Oki, Japan earthquake and the 2010 El-Mayor Cucapah earthquake. But all ground motions recorded with high-rate GPS to date have been far-field or had small static offsets making high-rate GPS currently of limited value, but with potential to produce useful data in the future.

We defined a functional form for fling and extracted fling pulses from all ground motions in our compiled dataset using the pattern search global optimization algorithm. We then derived a predictive model for fling parameters from the extracted pulses and compared it to existing empirical models. There are only two empirical models explicitly for fling [7, 8], but relevant empirical models exist for pulse period [e.g., 34, 35], surface displacement as a function of distance from the fault for the 1906 San Francisco earthquake [36], and surface displacement along the fault [e.g., 37].

In general for all compiled data, the median pulse period scaled with magnitude as expected, though the distribution of pulse periods for SF scenarios (large magnitude) contained fewer short-periods than some predictions. For all simulations that were surface-rupturing, the fling amplitude scaled with distance according to Abrahamson [7], Kamai et al. [8], and Burks and Baker. The average surface fault displacement matched predictions from all fling models and the maximum surface fault displacement matched predictions from Wells and Coppersmith [37]. For ground motions within 10 km of the fault, plausible values of fling amplitude range from 0.05 to 10 m, depending on magnitude and slip distribution on the fault, and fling periods range from 1 to 20 s.

The presence of fling in strong ground motions has been largely ignored

by engineers because recordings are typically corrected for errors via a combination of filtering and baseline correction, which removes static offsets. But with new data sources becoming available, such as ground motion simulations and high-rate GPS, the amount of data available to characterize fling is growing, although these data sources are still developing. Ground motion simulations are rapidly changing based on developments in seismology, and they are just now starting to undergo rigorous validation for engineering applications. And high-rate GPS has not yet recorded many near-field ground motions with large static offsets. But these data sources will likely be useful for characterizing fling in the future, and more data may lead to more concrete conclusions about the effect of fling on structural response.

## 6. Acknowledgements

This research was supported by the Southern California Earthquake Center (SCEC). SCEC is funded by NSF Cooperative Agreement EAR-1033462 and USGS Cooperative Agreement G12AC20038. The SCEC contribution number for this paper is 1964. The authors would like to thank Albert Kottke and PEER for sharing the reverse scenario simulations, Brad Aagaard and the USGS for sharing the low-frequency simulations of the 1906 San Francisco earthquake and several scenarios on the Hayward fault, Walt Silva and PE&A for sharing their database of baseline corrected ground motions, Erol Kalkan for sharing his unprocessed ground motions from the 1999 Kocaeli, Turkey earthquake, and Kristine Larson for sharing combined strong motion and high-rate GPS recordings from the 2003 Tokachi-Oki, Japan earthquake. This work could not have been completed without their generous sharing of data.

## References

- [1] Bolt B, Abrahamson N. Estimation of strong seismic ground motion. In: International Handbook of Earthquake and Engineering Seismology; vol. 81B. Academic Press; 2003, p. 983–1001.
- [2] Boore DM, Bommer JJ. Processing of strong-motion accelerograms: needs, options and consequences. *Soil Dynamics and Earthquake Engineering* 2005;25(2):93–115.

- [3] Boore DM. Effect of baseline corrections on displacements and response spectra for several recordings of the 1999 Chi-Chi, Taiwan, earthquake. *Bulletin of the Seismological Society of America* 2001;91(5):1199–211.
- [4] Akkar S, Boore DM. On baseline corrections and uncertainty in response spectra for baseline variations commonly encountered in digital accelerograph records. *Bulletin of the Seismological Society of America* 2009;99(3):1671–90.
- [5] Alavi B, Krawinkler H. Effects of near-fault ground motions on frame structures. Tech. Rep. 138; Blume Earthquake Engineering Center; Stanford, CA; 2001.
- [6] Kalkan E, Kunnath SK. Effects of fling step and forward directivity on seismic response of buildings. *Earthquake Spectra* 2006;22(2):367–90.
- [7] Abrahamson NA. Velocity pulses in near-fault ground motions. In: *Proceedings of the UC Berkeley - CUREE Symposium in Honor of Ray Clough and Joseph Penzien*. Berkeley, California; 2002, p. 40–1.
- [8] Kamai R, Abrahamson N, Graves R. Adding fling effects to processed ground-motion time histories. *Bulletin of the Seismological Society of America* 2014;104(4):1914–29.
- [9] Michel R, Avouac JP, Taboury J. Measuring near field coseismic displacements from SAR images: Application to the Landers earthquake. *Geophysical Research Letters* 1999;26(19):3017–20.
- [10] Simons M, Fialko Y, Rivera L. Coseismic deformation from the 1999 Mw 7.1 Hector Mine, California, earthquake as inferred from InSAR and GPS observations. *Bulletin of the Seismological Society of America* 2002;92(4):1390–402.
- [11] Burks LS. Ground motion simulations: Validation and application for civil engineering problems. Ph.D.; Stanford University; Stanford, CA; 2014.
- [12] Chiou B, Darragh R, Gregor N, Silva W. NGA project strong-motion database. *Earthquake Spectra* 2008;24(1):23–44.

- [13] Ancheta TD, Darragh RB, Stewart JP, Seyhan E, Silva WJ, Chiou BSJ, et al. PEER NGA-West2 database. Tech. Rep. PEER 2013/03; Pacific Earthquake Engineering Research Center; Berkeley, CA; 2013.
- [14] CESMD . Center for engineering strong motion data. 2012. URL [www.strongmotioncenter.org](http://www.strongmotioncenter.org).
- [15] Haddadi H, Shakal A, Huang M, Parrish J, Stephens C, Savage W, et al. Report on progress at the center for engineering strong motion data (CESMD). In: 15th World Conference on Earthquake Engineering. Lisbon, Portugal; 2012, p. 1–7.
- [16] Ambraseys N, Smit P, Douglas J, Margaritis B, Sigbjornsson R, Olafsson S, et al. Internet site for European strong-motion data. *Bollettino di Geofisica Terorica ed Applicata* 2004;45(3):113–29.
- [17] Luzi L, Hailemikael S, Bindi D, Pacor F, Mele F, Sabetta F. ITACA (ITalian ACcelerometric Archive): a web portal for the dissemination of Italian strong-motion data. *Seismological Research Letters* 2008;79(5):716–22.
- [18] Pacor F, Paolucci R, Luzi L, Sabetta F, Spinelli A, Gorini A, et al. Overview of the Italian strong motion database ITACA 1.0. *Bulletin of Earthquake Engineering* 2011;9(6):1723–39.
- [19] Chen X. Near-field ground motion from the landers earthquake. Tech. Rep. EERL 95-02; Earthquake Engineering Research Laboratory; California Institute of Technology; 1995.
- [20] Iwan WD, Moser MA, Peng CY. Some observations on strong-motion earthquake measurement using a digital accelerograph. *Bulletin of the Seismological Society of America* 1985;75(5):1225–46.
- [21] Wu YM, Wu CF. Approximate recovery of coseismic deformation from Taiwan strong-motion records. *Journal of Seismology* 2007;11:159–70.
- [22] Douglas J, Aochi H. A survey of techniques for predicting earthquake ground motions for engineering purposes. *Surveys in Geophysics* 2008;29(3):187–220.

- [23] Aagaard BT, Brocher TM, Dolenc D, Dreger D, Graves RW, Harmsen S, et al. Ground-motion modeling of the 1906 San Francisco earthquake, part I: validation using the 1989 Loma Prieta earthquake. *Bulletin of the Seismological Society of America* 2008;98(2):989–1011.
- [24] Aagaard BT, Brocher TM, Dolenc D, Dreger D, Graves RW, Harmsen SC, et al. Ground-motion modeling of the 1906 San Francisco earthquake, part II: ground-motion estimates for the 1906 earthquake and scenario events. *Bulletin of the Seismological Society of America* 2008;98(2):1012–46.
- [25] Aagaard BT, Graves RW, Schwartz DP, Ponce DA, Graymer RW. Ground-motion modeling of Hayward fault scenario earthquakes, part 1: Construction of the suite scenarios. *Bulletin of the Seismological Society of America* 2010;100(6):2927–44.
- [26] Aagaard BT, Graves RW, Rodgers A, Brocher TM, Simpson RW, Dreger D, et al. Ground-motion modeling of Hayward fault scenario earthquakes, part II: simulation of long-period and broadband ground motions. *Bulletin of the Seismological Society of America* 2010;100(6):2945–77.
- [27] Graves RW, Pitarka A. Broadband ground-motion simulation using a hybrid approach. *Bulletin of the Seismological Society of America* 2010;100(5A):2095–123.
- [28] SCEC . Broadband Platform. 2012. URL [http://scec.usc.edu/scecpedia/Broadband\\_Platform](http://scec.usc.edu/scecpedia/Broadband_Platform).
- [29] Miyazaki S, Larson KM, Choi K, Hikima K, Koketsu K, Bodin P, et al. Modeling the rupture process of the 2003 september 25 Tokachi-Oki (Hokkaido) earthquake using 1-Hz GPS data. *Geophysical Research Letters* 2004;31(21).
- [30] Ji C, Larson KM, Tan Y, Hudnut KW, Choi K. Slip history of the 2003 San Simeon earthquake constrained by combining 1-Hz GPS, strong motion, and teleseismic data. *Geophysical Research Letters* 2004;31.
- [31] Emore GL, Haase JS, Choi K, Larson KM, Yamagiwa A. Recovering seismic displacements through combined use of 1-hz gps and strong-

- motion accelerometers. *Bulletin of the Seismological Society of America* 2007;97(2):357–78.
- [32] Bock Y, Melgar D, Crowell BW. Real-time strong-motion broadband displacements from collocated GPS and accelerometers. *Bulletin of the Seismological Society of America* 2011;101(6):2904–25.
- [33] Lewis RM, Shepherd A, Torczon V. Implementing generating set search methods for linearly constrained minimization. *SIAM Journal on Scientific Computing* 2007;29(6):2507–30.
- [34] Bray JD, Rodriguez-Marek A. Characterization of forward-directivity ground motions in the near-fault region. *Soil Dynamics and Earthquake Engineering* 2004;24(11):815–28.
- [35] Shahi SK, Baker JW. An empirically calibrated framework for including the effects of near-fault directivity in probabilistic seismic hazard analysis. *Bulletin of the Seismological Society of America* 2011;101(2):742–55.
- [36] Byerley P, DeNoyer J. Energy in earthquakes as computed from geodetic observations. In: Benioff H, Ewing M, Howell BF, Press F, editors. *Contributions in Geophysics in Honor of Beno Gutenberg*. New York: Pergamon Press; 1958, p. 17–35.
- [37] Wells DL, Coppersmith KJ. New empirical relationships among magnitude, rupture length, rupture width, rupture area, and surface displacement. *Bulletin of the Seismological Society of America* 1994;84(4):974–1002.
- [38] Somerville PG. Development of an improved representation of near fault ground motions. In: *Seminar on Utilization of Strong-Motion Data*. Oakland, CA; 1998, p. 1–20.
- [39] Somerville P, Irikura K, Graves R, Sawada S, Wald D, Abrahamson N, et al. Characterizing crustal earthquake slip models for the prediction of strong ground motion. *Seismological Research Letters* 1999;70(1):59–80.